AIP | APL Materials

Enhanced 77 K vortex-pinning in Y Ba2Cu3O7−x films with Ba2Y TaO6 and mixed Ba2Y TaO6 + Ba2Y NbO6 nano-columnar inclusions with irreversibility field to 11 T

F. Rizzo, A. Augieri, A. Angrisani Armenio, V. Galluzzi, A. Mancini, V. Pinto, A. Rufoloni, A. Vannozzi, M. Bianchetti, A. Kursumovic, J. L. MacManus-Driscoll, A. Meledin, G. Van Tendeloo, and G. Celentano

Citation: APL Mater. **4**, 061101 (2016); doi: 10.1063/1.4953436
View online: http://dx.doi.org/10.1063/1.4953436
View Table of Contents: http://scitation.aip.org/content/aip/journal/aplmater/4/6?ver=pdfcov
Published by the AIP Publishing

Enhanced 77 K vortex-pinning in $YBa_2Cu_3O_{7-x}$ films with Ba_2YTaO_6 and mixed Ba_2YTaO_6 + Ba_2YNbO_6 nano-columnar inclusions with irreversibility field to 11 T

F. Rizzo,[1] A. Augieri,[1] A. Angrisani Armenio,[1] V. Galluzzi,[1] A. Mancini,[1] V. Pinto,[1] A. Rufoloni,[1] A. Vannozzi,[1] M. Bianchetti,[2] A. Kursumovic,[2] J. L. MacManus-Driscoll,[2] A. Meledin,[3] G. Van Tendeloo,[3] and G. Celentano[1]
[1]*ENEA, Frascati Research Centre, Via E. Fermi, 45, 00044 Frascati, Italy*
[2]*Department of Materials Science and Metallurgy, University of Cambridge, 27 Charles Babbage Rd., Cambridge CB3 0FS, United Kingdom*
[3]*EMAT Research Group, University of Antwerp, Groenenborgerlaan 171, 2020 Antwerp, Belgium*

(Received 13 April 2016; accepted 23 May 2016; published online 8 June 2016)

Pulsed laser deposited thin $YBa_2Cu_3O_{7-x}$ (YBCO) films with pinning additions of 5 at. % Ba_2YTaO_6 (BYTO) were compared to films with 2.5 at. % Ba_2YTaO_6 + 2.5 at. % Ba_2YNbO_6 (BYNTO) additions. Excellent magnetic flux-pinning at 77 K was obtained with remarkably high irreversibility fields greater than 10 T (YBCO-BYTO) and 11 T (YBCO-BYNTO), representing the highest ever achieved values in YBCO films. [http://dx.doi.org/10.1063/1.4953436]

TEM analysis revealed straight and continuous nano-rods with mean diameter 5 nm and density 2500 μm^{-2}. In the YBCO-BYNTO films, a large number of Y_2O_3 nanoparticles dispersed in the YBCO matrix close to the BYNTO nanocolumns were observed while partly interrupted BYTO nanocolumns with hammerhead-like ends were recognized in YBCO-BYTO films.

The introduction of ordered nanosized oxide secondary phases in epitaxial thin films has lately attracted a large interest in several areas of materials science. In fact, the growth of self-assembled columnar nanostructures embedded into epitaxial thin films, allowing the tuning of the material functionalities, has opened unprecedented prospects for potential applications in ferroelectrics, thermoelectrics, and magnetoelectrics devices and high temperature superconductors.[1–5]

In particular, the possibility to strongly improve flux pinning in $YBa_2Cu_3O_{7-x}$ films by introducing nano-scale artificial pinning centres (APCs) has attracted a remarkable interest in recent years. In fact, by enhancing the transport film performances as a function of both the applied magnetic field intensity and the direction, it is possible to reach the current requirements needed in a wide range of present and future applications.[6] In particular, the realisation of superconducting tapes able of carrying high current in high magnetic field is essential in view of both power and magnet applications to enable them to operate at 77 K, i.e., transformers, motors, and generators where current performance is insufficient at this temperature.[7–9]

Since the first demonstration of $BaZrO_3$ (BZO) nanoinclusion defect pinning,[10] several nano-scale pinning compositions and structures have been studied over different temperature and magnetic field regimes.[11–15] In particular, the double perovskite-like Ba_2YTaO_6 (BYTO) and Ba_2YNbO_6 (BYNO) have been reported as very effective pinning sources either as single secondary phases or as simultaneous doping of BYTO + BYNO (BYNTO).[16–19] More recently, high growth rate YBCO-BYNO and YBCO-BYNTO films have shown very good J_c performance at 77 K and in intermediate field regimes,[20] and for YBCO-BYNTO, vortex pinning remains very effective in an extended range of temperature and magnetic field.[21,22] The irreversibility field, H_{irr}, values at 77 K have been increased towards 10 T. However, the question is whether this can be improved further.

In this paper, the J_c behaviour of YBCO-BYTO (5 at. %) and YBCO-BYNTO (2.5 at. % BYTO + 2.5 at. % BYNO) films was investigated at liquid nitrogen temperature in magnetic field regimes up to 12 T and compared with the J_c behaviour of an optimised pure YBCO film. For both pinning combinations, a remarkable improvement of J_c with respect to pristine YBCO was observed, as well as very high irreversibility field values and maximum pinning force density. Also, in the field range [0.1–5] T (5 T being the highest field measured), superior angular behaviour of J_c was observed consistent with very well defined *c*-axis oriented BYTO/BYNTO nanocolumns observed in the YBCO matrix. Additionally, for the YBCO-BYNTO films, the J_c is strongly enhanced in the mid-to-high field regime.

Mixed targets of YBCO with double perovskite-like BYTO and BYNTO were used to grow composite YBCO films on $SrTiO_3$ (STO) single-crystal substrates by pulsed laser deposition. In brief, targets were prepared by mixing and grinding the precursor oxides BaO, Y_2O_3, and Nb/Ta_2O_5 in stoichiometric quantities with pure YBCO powder and sintering in flowing oxygen at 950 °C. Targets so obtained were ablated using laser (308 nm) with fluence of ~2 J/cm^2 (10 Hz repetition rate). The thickness of the films was ~230 nm as estimated by cross section TEM analysis (bright field TEM (BF TEM) and high angle annular dark field scanning TEM (HAADF STEM)) from which a film growth rate of ~0.3 nm/s was derived. TEM cross section analysis allowed us to visualise the BYTO/BYNTO nano-inclusions in the YBCO matrix and to estimate their morphology (average size, density, linearity, and distribution). *DC* transport J_c measurements were carried out on 30-50 μm wide and 1 mm long strips. The films were mounted on a rotating sample holder in a cryostat equipped with a 12 T superconducting magnet in order to record J_c as a function of the magnetic field intensity and orientation always keeping the current normal to the field direction (maximum Lorentz force configuration). All J_c values were determined with the 1 μV cm^{-1} electric field criterion.

The structural TEM investigation highlights the nanocolumnar *c*-axis oriented growth of the artificial pinning centres (APCs) and secondary phases in both the films. The cross section images in Fig. 1 compares the YBCO-BYTO ((a) and (c)) and YBCO-BYNTO ((b), (e), and (f)) morphology. Both films have a thickness of about 215-230 nm and show a clear *c*-axis oriented nanocolumnar growth, which starts over a thin layer of distorted YBCO at the interface with the STO substrate and runs straight through the YBCO layer (Figs. 1(a) and 1(b)).

This continuous growth of the nanocolumn pinning centres was initially observed in YBCO films with the addition of rare earth tantalate nanoparticles to the YBCO target.[16] The pinning centres were identified to be double perovskite, $Ba_2(ReY)TaO_6$ (BRETO).[17] In those cases, Gd, Er, and Yb were used as rare earth elements. However Y was not studied. Recently, continuous nanocolumns running through the entire YBCO film have also been reported for the $Ba_2Y(Nb,Ta)O_6$ nanocolumns.[22]

Despite a general similarity between the BYTO and BYNTO growth in the YBCO matrix, some major differences are distinctly visible in Fig. 1. In the YBCO-BYTO film, the BYTO columns have a mean diameter d_{BYTO} of ~5 nm and a density n_{BYTO} ~ 2500 μm^{-2}. However, some localised areas of the film show nanocolumns interrupted by the YBCO matrix (see yellow dotted lines in Figs. 1(a) and 1(c)). In these areas, the BYTO nanocolumns stop at the same height and have a hammerhead-like structure on their top with a diameter of about 10-35 nm (red arrows in Fig. 1(c) and the magnified hammerhead in inset Fig. 1(d)) with extension along the *a*-*b* plane of several hundreds of nanometers. The thickness of these layers is between 10 and 40 nm, and on top of the layers, the columnar self-organised growth of BYTO resumes. As revealed by the energy dispersive X-ray analysis (Figure S3 of the supplementary material[23]), the hammerhead-like structures are entirely composed of BYTO, contrary to similar truncation effects with Y_2O_3 nanoparticles reported in YBCO with columnar APCs.[24]

In addition, several short double Cu–O chain intergrowths are observed between the columns in the YBCO matrix. This locally creates $YBa_2Cu_4O_{8-x}$ (Y124) or $Y_2Ba_4Cu_7O_{15-x}$ (Y247) type structures. These intergrowths are mainly located in 3 different areas: near the interface between the STO substrate and the YBCO, in regions between the BYTO columns, and on the top of the hammerhead-like structures (Figure S4 of the supplementary material[23]). The presence of these intergrowths can be induced by the mismatch between the YBCO and the APCs lattice, creating a strain field in the YBCO matrix. In the thinner regions of the TEM lamella, the samples are slightly bent near the interface and

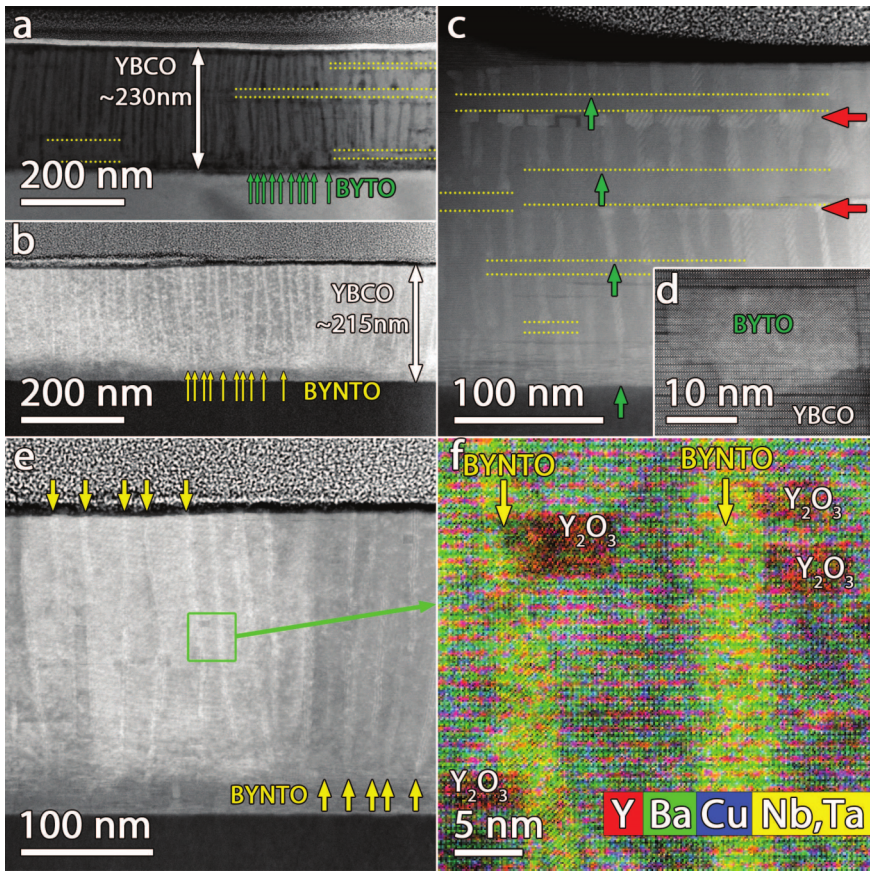

FIG. 1. TEM cross section images of the YBCO-BYTO ((a), (c), and (d)) and YBCO-BYNTO ((b), (e), and (f)) films. (a) A BF-TEM image while ((b)-(e)) are ADF STEM images. The vertical green and yellow arrows highlight the BYTO and BYNTO nanocolumns, respectively. The horizontal red arrows indicate the hammerhead-like ends of the truncated BYTO nanocolumns (c). One of the hammerheads is magnified in inset (d). The dotted yellow lines in (a) and (c) point at the nanocolumn interruption and define the BYTO-free YBCO regions. Part label (a) shows that the column truncation is not a local phenomenon; it occurs in different areas of the sample (top and bottom). The EDX map in (f) is from the green area in (e); it accentuates the presence of Y_2O_3 nanoparticles close to the BYNTO nanocolumns.

therefore one could argue that the presence of the intergrowths is induced by sample preparation. However also the thicker regions contain a number of Y124/Y247 intergrowths. This is a strong argument that the intergrowths are intrinsic and not induced by sample manipulation.

An increase of the nanocolumn length might cause an increase of the stress cumulated between the columns and the surrounding YBCO matrix. Part of the total stress in the YBCO-BYTO films is certainly relaxed by the presence of interface misfit dislocations and the formation of several intergrowths, as shown by the TEM investigation. However, a large number of such defects, which are rich in Cu–O layers with respect to YBCO, might induce an excess of Y and Ba which may lead to an enlargement of the column, thus generating the hammerheads. At the same time, this increase in the column diameter increases the cumulated stress up to a level, which prevents further growth of the hammerheads. The only way to re-establish the proper growth is to stop the nanocolumn growth, i.e., to truncate.

The BYNTO columns in the YBCO-BYNTO films show a similar mean diameter as the BYTO columns; about $d_{\mathrm{BYNTO}} \sim 5$ nm and a similar density n_{BYNTO} of ~2500 $\mu\mathrm{m}^{-2}$. Different from the BYTO system, the BYNTO columns are continuous and one dimensional in the YBCO matrix without any sign of segmentation (Figs. 1(b) and 1(e)). Moreover, in the YBCO-BYNTO films, Y_2O_3 nanoparticles are present close to the BYNTO nanocolumns; this is confirmed by energy dispersive X-ray spectroscopy (EDX) (Fig. 1(f)) in agreement with previous observations.[20,22] These Y_2O_3 nanoparticles are not present in the BYTO case. Hence, the simultaneous availability

of two kinds of ions (Nb^{5+} and Ta^{5+}) leads to a different growth process. In fact, the melting point of Nb_2O_5 (1512 °C) is lower than the corresponding one of Ta_2O_5 (1872 °C), leading to a greater mobility of Nb^{5+} ions with respect to Ta^{5+} ions at the typical YBCO deposition temperatures.[25] Therefore, the availability of faster diffusing Nb^{5+} ions in the BYNTO structures allows self-organised growth to be achieved, thus locally relaxing the strain field without a strong need of generating intergrowths. Hence, this situation favours a growth without any column truncation.

In Fig. 2 (top), the critical current densities $J_c(B)$ are shown at $T = 77$ K as a function of the applied magnetic field H ($B = \mu_0 H$) with $H \parallel c$-axis of the films. Data refer to YBCO-BYTO

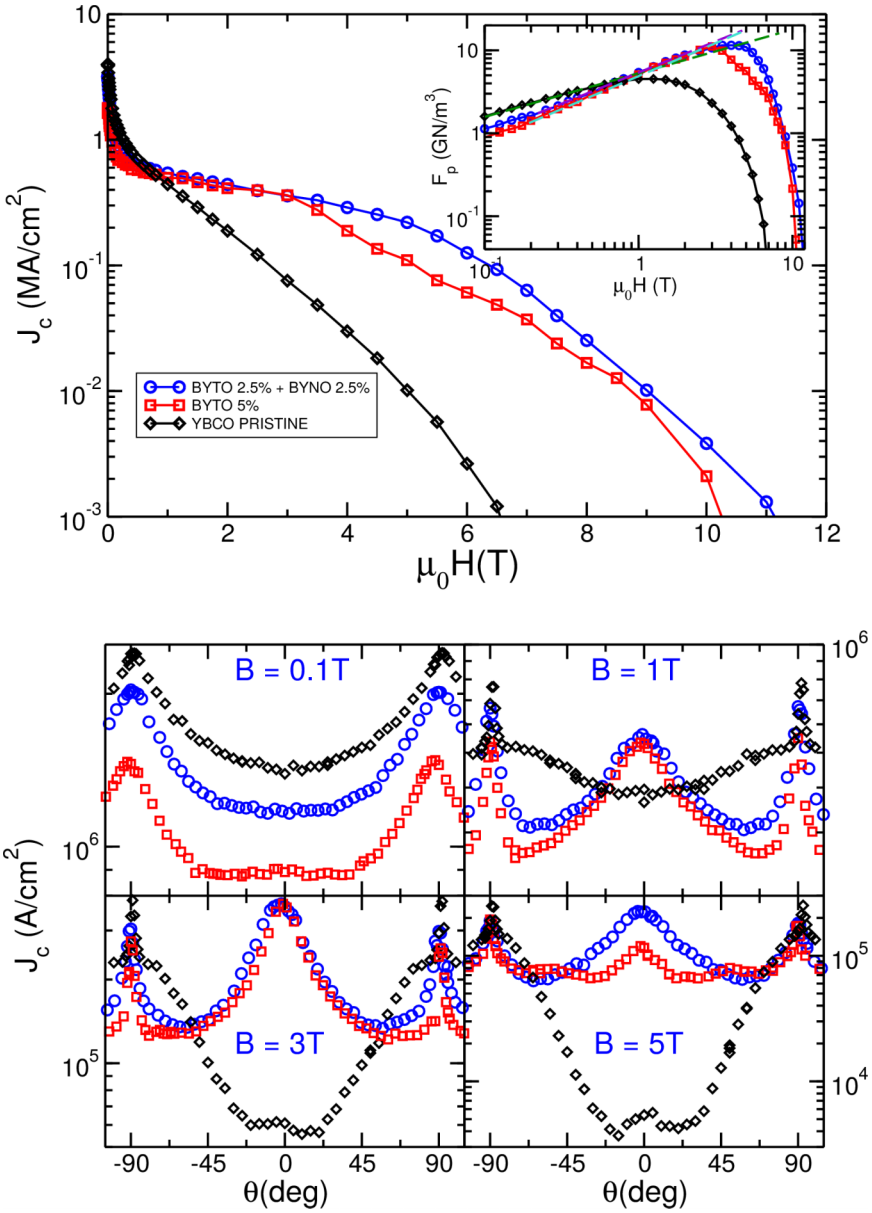

FIG. 2. (Top) Critical current density as a function of the applied magnetic field recorded for YBCO-BYTO (red squares), YBCO-BYTO + BYNO (blue circles), and pristine YBCO (black diamonds) films at 77 K. In the inset is highlighted the pinning force densities as a function of the applied field recorded for YBCO-BYNTO. Dashed lines show the power law behaviour $F_p \sim H^{1-\alpha}$ for YBCO-BYNTO (violet), YBCO-BYTO (turquoise), and pristine YBCO (green). (Bottom) Critical current density as a function of the applied field direction (0° corresponds to B ∥ film c-axis) for the pristine YBCO (black diamonds), YBCO-BYTO (red squares), and YBCO-BYNTO (blue circles) at 77 K and magnetic field values of 0.1, 1, 3, and 5 T.

(red squares), YBCO-BYNTO (blue circles), and YBCO pristine (black diamonds). Both the YBCO-BYTO and YBCO-BYNTO films exhibit a superior in-field behaviour of the critical current density J_c in the mid-to-high magnetic field range B = [1–12] T with respect to the pristine YBCO film. The observed J_c improvements are in agreement with enhanced performances previously reported for tantalate additions[16] which give fine straight columns and mixed tantalate/niobate additions,[20] which give highly linear segmented columns. As far as tantalate columns with mixed rare earths goes, namely, $Ba_2(Y/Gd)TaO_6$,[17] the J_c at 77 K is lower than what is measured for pure BYTO as shown in Fig. 2, although the mixed rare earth samples were thicker, at 800 nm, and also were grown on buffered metal substrates and hence a clear comparison cannot be made directly.

As seen in Fig. 2 (top), in the mid-field regime B = [1–3.5] T, the critical current densities of the YBCO films with both BYTO and BYNTO APCs show values close each other with similar in-field behaviours with an extended plateau. At about 3.5 T, the J_c of YBCO-BYTO film shows a kink with a pronounced drop with respect to the previous plateau. On the other hand, the YBCO-BYNTO film shows a more gradual drop, at a higher field value of around 5 T. From the evaluated column density n, an *equivalent* or *matching field* (magnetic field value as vortex density matches the defects density) can be evaluated by using $B_\phi = n\phi_0$, where ϕ_0 is the magnetic flux quantum and thus both YBCO films have a similar value $B_\phi \sim 5.2$ T. Accordingly, in the YBCO-BYNTO film, the drop-off from the plateau-like behaviour at 5 T can be explained in terms of a matching field effect.[26] A similar J_c behaviour was also observed for linear segmented nanorods formed by $Ba_2(Y/Gd)(Ta/Nb)O_6$[20,22] even though in a narrower B range with the lower matching field B_ϕ = 2.6 T evaluated. The lower-field drop (3.5 T) for the YBCO-BYTO film can be explained by the partial truncation of the BYTO nanocolumns, bringing less effective pinning of the vortices with respect to the continuous linear defects found in YBCO-BYNTO.

The comparison between the pinning force density $F_p = J_c \times B$ at 77 K is shown in the inset of Fig. 2 (top). Both YBCO-BYTO and YBCO-BYNTO exhibit higher F_p values with respect to the pristine YBCO film in the mid-to-high field regime, 1 T < B < 12 T.

In Table I, the 77 K self-field critical current density $J_c(0)$, irreversibility field B_{irr} (evaluated by using the criterion $F_p(B_{irr}) = F_p^{Max}/100$), maximum pinning force density F_p^{Max}, and α parameter evaluated in the low field regime in which the critical current density shows a power law decay $J_c \sim H^{-\alpha}$[27] are reported for the three different films.

Both the YBCO films containing the APCs show a notable increase in the irreversibility field B_{irr} and in the maximum pinning force density F_p^{Max} with respect to high quality pristine YBCO. These irreversibility field values above 10 T are among the best ever recorded at 77 K, whereas greater F_p^{Max} values at 77 K have already been reported for YBCO films with niobates and tantalates columns.[20,28] The YBCO-BYNTO film exhibits the best performance in terms of B_{irr} and F_p^{Max} while the values of the α parameter are the same for both APCs in the range 0.2-0.3. These low α values are characteristic of a strong correlated pinning contribution[27] consistent with the well-defined nanocolumnar growth highlighted in Fig. 1.

Angular transport measurements were undertaken in order to evaluate the effectiveness of the correlated pinning contribution arising from the BYTO/BYNTO nanocolumnar growth. Therefore, the critical current density behaviour was evaluated as a function of the applied magnetic field direction at T = 77 K, as shown in Fig. 2 (bottom). Both the YBCO-BYTO and YBCO-BYNTO present a clear correlated pinning contribution with respect to the pristine YBCO, with a significant enhancement of J_c in the mid-to-high magnetic field range B = [1–5] T, when the applied magnetic field is parallel to the nanocolumns. However, some differences arise between the J_c

TABLE I. Irreversibility fields, maximum of the pinning force densities, and values of the α parameter for the films of YBCO + APCs and for a high quality pristine YBCO grown under optimised deposition conditions.

T = 77 K	$J_c(0)$ (MA/cm^2)	B_{irr} (T)	F_p^{Max} (GN/m^3)	α
Pristine YBCO	4.0	6.8	4.5	0.52
YBCO-BYTO	1.6	10.23	9.1	0.23
YBCO-BYNTO	3.2	11.12	11.5	0.30

in-field angular behaviour of YBCO-BYTO and YBCO-BYNTO. First, at low field (B = 0.1 T), consistent with the in-field critical current densities shown in Fig. 6, even if the magnitude of J_c in YBCO-BYTO is lower than J_c in YBCO-BYNTO and pristine YBCO (due to a marked presence of intergrowths which ruin the YBCO matrix), the correlated pinning mechanism of YBCO-BYTO is the most effective, giving rise to an almost flat J_c angular dependence in a wider angular range ($\theta \sim [-45°$ to $45°]$) with respect to YBCO-BYNTO.

In the mid-field range, B = [1–3] T, the J_cs of the YBCO-BYTO and YBCO-BYNTO samples exhibits a similar correlated peak. In addition, increasing the field up to 3 T, the $\theta = 0°$ peak noticeably increases with respect to the J_c of the pristine YBCO. However, at high field (B = 5 T), the correlated peak in YBCO-BYNTO is clearly more effective than the corresponding peak in YBCO-BYTO. This feature is consistent with Figure 2, which showed that nanocolumn density is not the only important factor controlling the field dependent behaviour of J_c but also that the continuity controls the high-field behaviour, continuous columns being important for pinning at high fields.

In the high field range ($B \geq 5$ T), the J_c angular behaviours for both the YBCO-BYTO and YBCO-BYNTO films are more flat than J_c in the pristine YBCO film, indicating that the vortex pinning mechanisms are active in an extended angular interval. In addition, as can be seen from the curves at 1 T, 3 T, and 5 T, the J_c values for $H \parallel (a, b)$ planes ($\theta = \pm 90°$) do not exhibit any remarkable degradation with respect to the pristine YBCO film, thus both the BYTO and BYNTO columnar structures preserve the YBCO intrinsic pinning properties. Similar flat angular behaviour was observed in YBCO films with tantalate added films previously.[16,28]

A substantial improvement of the in-field and angular critical currents at 77 K was obtained for YBCO films with Ba_2YTaO_6 and Ba_2YTaO_6 + Ba_2YNbO_6 nano-columnar inclusions with respect to an optimised pristine YBCO film. The YBCO films with artificial pinning centres, grown by pulsed laser deposition on $SrTiO_3$ single crystals, showed excellent in-field behaviours of the critical current density with remarkably high irreversibility fields greater than 10 T and 11 T, respectively, in YBCO-BYTO and in YBCO-BYNTO. Both YBCO + APCs films, grown under similar optimised deposition conditions, presented similar nanocolumn distances and mean diameters. However, a detailed TEM structural analysis underlined some of the key differences in the pinning landscapes of the two films. In particular, while nanocolumns of the YBCO-BYNTO film extend straight and with continuity along the whole film, in some areas of the YBCO-BYTO film, the nanocolumns are truncated. As a consequence, different behaviours for the angular dependence of the critical current densities were observed at 77 K.

Both film compositions showed a superior angular behaviour of the critical current density with respect to high quality, pristine YBCO film with a strong correlated peak corresponding to $B \parallel c$-axis noticeable in the intermediate field range B = [1–3] T. However, at higher fields (3–5 T), the correlated peak in the angular behaviour of J_c in YBCO-BYNTO was clearly more effective than the corresponding peak in YBCO-BYTO. In any case, both films showed a superior angular behaviour of the critical current density with respect to a high quality pristine YBCO film. Overall, both BYTO and BYTO-BYNO inclusions are very efficient pinning solutions for the realization of high quality coated conductors, particularly for high fields (B $\geq$ 3 T).

This work was financially supported by EUROTAPES, a collaborative project funded by the European Commission's Seventh Framework Program (FP7/2007-2013) under Grant Agreement No. 280432.

[1] S. Lee, A. Sangle, P. Lu, A. Chen, W. Zhang, J. S. Lee, H. Wang, Q. Jia, and J. L. MacManus-Driscoll, "Novel electroforming-free nanoscaffold memristor with very high uniformity, tunability, and density," Adv. Mater. **26**, 6284–6289 (2014).
[2] A. Chen, W. Zhang, F. Khatkatay, Q. Su, C.-F. Tsai, L. Chen, Q. X. Jia, J. L. Macmanus-Driscoll, and H. Wang, "Magneto-transport properties of quasi-one-dimensionally channeled vertically aligned heteroepitaxial nanomazes," Appl. Phys. Lett. **102**, 093114 (2013).
[3] A. Chen, M. Weigand, Z. Bi, W. Zhang, X. Lü, P. Dowden, J. L. Macmanus-Driscoll, H. Wang, and Q. Jia, "Evolution of microstructure, strain and physical properties in oxide nanocomposite films," Sci. Rep. **4**, 5426 (2014).
[4] T. Fix, E.-M. Choi, J. W. A. Robinson, S. B. Lee, A. Chen, B. Prasad, H. Wang, M. G. Blamire, and J. L. Macmanus-Driscoll, "Electric-field control of ferromagnetism in a nanocomposite via a ZnO phase," Nano Lett. **13**(12), 5886–5890 (2013).
[5] S. H. Wee, Y. Gao, Y. L. Zuev, K. L. More, J. Meng, J. Zhong, G. M. Stocks, and A. Goyal, "Self-assembly of nanostructured, complex, multication films via spontaneous phase separation and strain-driven ordering," Adv. Funct. Mater. **23**, 1912–1918 (2013).

[6] X. Obradors and T. Puig, "Coated conductors for power applications: Materials challenges," Supercond. Sci. Technol. **27**, 044003 (2014).
[7] M. Noe and M. Steurer, "High-temperature superconductor fault current limiters: Concepts, applications, and development status," Supercond. Sci. Technol. **20**, R15–R29 (2007).
[8] P. Tixador, "Development of superconducting power devices in Europe," Physica C **470**, 971–979 (2010).
[9] L. Muzzi, G. De Marzi, A. Di Zenobio, and A. della Corte, "Cable-in-conduit conductors: Lessons from the recent past for future developments with low and high temperature superconductors," Supercond. Sci. Technol. **28**, 053001 (2015).
[10] J. L. MacManus-Driscoll, S. R. Foltyn, Q. X. Jia, H. Wang, A. Serquis, L. Civale, B. Maiorov, M. E. Hawley, M. P. Maley, and D. E. Peterson, "Strongly enhanced current densities in superconducting coated conductors of $YBa_2Cu_3O_{7-x}$ + $BaZrO_3$," Nat. Mater. **4**, 439–443 (2004).
[11] P. Mele, K. Matsumoto, T. Horide, A. Ichinose, M. Mukaida, Y. Yoshida, S. Horii, and R. Kita, "Ultra-high flux pinning properties of $BaMO_3$-doped $YBa_2Cu_3O_{7-x}$ thin films (M = Zr, Sn)," Supercond. Sci. Technol. **21**, 032002 (2008).
[12] K. Matsumoto and P. Mele, "Artificial pinning center technology to enhance vortex pinning in YBCO coated conductors," Supercond. Sci. Technol. **23**, 014001 (2010).
[13] B. Maiorov *et al.*, "Synergetic combination of different types of defect to optimize pinning landscape using $BaZrO_3$-doped $YBa_2Cu_3O_7$," Nat. Mater. **8**, 398 (2009).
[14] J. Gutiérrez *et al.*, "Strong isotropic flux pinning in solution-derived $YBa_2Cu_3O_{7-x}$ nanocomposite superconductor films," Nat. Mater. **6**, 367–373 (2007).
[15] C.-F. Tsai, L. Chen, A. Chen, F. Khatkhatay, W. Zhang, and H. Wang, "Enhanced flux pinning properties in self-assembled magnetic $CoFe_2O_4$ nanoparticles doped $YBa_2Cu_3O_{7-\delta}$ thin films," IEEE Trans. Appl. Supercond. **23**(3), 8001204 (2013).
[16] S. A. Harrington, J. H. Durrell, B. Maiorov, H. Wang, S. C. Wimbush, A. Kursumovic, J. H. Lee, and J. L. MacManus-Driscoll, "Self-assembled, rare earth tantalate pyrochlore nanoparticles for superior flux pinning in $YBa_2Cu_3O_{7-\delta}$ films," Supercond. Sci. Technol. **22**, 022001 (2009).
[17] S. H. Wee, A. Goyal, E. D. Specht, C. Cantoni, Y. L. Zuev, V. Selvamanickam, and S. Cook, "Enhanced flux pinning and critical current density via incorporation of self-assembled rare-earth barium tantalate nanocolumns within $YBa_2Cu_3O_{7-\delta}$ films," Phys. Rev. B **81**, 140503(R) (2010).
[18] G. Ercolano, S. A. Harrington, H. Wang, C. F. Tsai, and J. L. MacManus-Driscoll, "Enhanced flux pinning in $YBa_2Cu_3O_{7-\delta}$ thin films using Nb-based double perovskite additions," Supercond. Sci. Technol. **23**, 022003 (2010).
[19] D. M. Feldmann *et al.*, "Improved flux pinning in $YBa_2Cu_3O_7$ with nanorods of the double perovskite Ba_2YNbO_6," Supercond. Sci. Technol. **23**, 095004 (2010).
[20] G. Ercolano, M. Bianchetti, S. C. Wimbush, S. A. Harrington, H. Wang, J. H. Lee, and J. L. MacManus-Driscoll, "State-of-the-art flux pinning in $YBa_2Cu_3O_{7-\delta}$ by the creation of highly linear, segmented nanorods of $Ba_2(Y/Gd)(Nb/Ta)O_6$ together with nanoparticles of $(Y/Gd)_2O_3$ an $(Y/Gd)Ba_2Cu_4O_8$," Supercond. Sci. Technol. **24**, 095012 (2011).
[21] F. Rizzo *et al.*, "Strong vortex pinning over wide temperature and field range in $YBa_2Cu_3O_{7-x}$ films with Ba_2YTaO_6 + Ba_2YNbO_6 inclusions grown over a range of deposition conditions in different laboratories" (unpublished).
[22] L. Opherden *et al.*, "Large pinning forces and matching effects in $YBa_2Cu_3O_{7-\delta}$ thin films with $Ba_2Y(Nb/Ta)O_6$ nano-precipitates," Sci. Rep. **6**, 21188 (2016).
[23] See supplementary material at http://dx.doi.org/10.1063/1.4953436 for surface (SEM) and structural analyses (XRD and additional TEM) of the YBCO-APC films.
[24] T. G. Holesinger *et al.*, "Nanorod self-assembly in high J_c $YBa_2Cu_3O_{7-x}$ films with Ru-Based double perovskites," Materials **4**, 2042 (2011).
[25] G. Ercolano *et al.*, "Strong correlated pinning at high growth rates in $YBa_2Cu_3O_{7-x}$ thin films with Ba_2YNbO_6 additions," J. Appl. Phys. **116**, 033915 (2014).
[26] A. Augieri, G. Celentano, V. Galluzzi, A. Mancini, A. Rufoloni, A. Vannozzi, A. Angrisani Armenio, T. Petrisor, L. Ciontea, S. Rubanov, E. Silva, and N. Pompeo, "Pinning analyses on epitaxial $YBa_2Cu_3O_{7-x}$ films with $BaZrO_3$ inclusions," J. Appl. Phys. **108**, 063906 (2010).
[27] A. Goyal *et al.*, "Irradiation-free, columnar defects comprised of self-assembled nanodots and nanorods resulting in strongly enhanced flux-pinning in $YBa_2Cu_3O_{7-\delta}$ films," Supercond. Sci. Technol. **18**, 1533 (2005).
[28] S. A. Harrington *et al.*, Nanotechnology **21**, 095604 (2010).